Dynamic Mechanical Properties of Polyurethane Elastomers Using a Nonmetallic Hopkinson Bar

S. RAO,[1] V. P. W. SHIM,[1] S. E. QUAH[2]

[1] Department of Mechanical & Production Engineering, National University of Singapore, Singapore 119260

[2] Motorola Electronics Pte. Ltd., 12, Ang Mo Kio St 64, Singapore 569088

Received 9 September 1996; accepted 20 February 1997

ABSTRACT: A modified split Hopkinson-bar apparatus, in which the striker and input/output bars are made of polycarbonate instead of metal, was used to study three typical examples of a high-density flexible polyurethane elastomer (PORON) in sheet form. This variation of the device reduces a mismatch in impedance between the input/output bars and the specimen, thus allowing the stress in the specimen to reach a uniform state before significant engineering strain is induced. Dynamic compressive stress–strain curves were obtained from the measured incident, transmitted, and reflected waves. This article presents the behavior of these foams as a function of strain rate; for PORON 4701-05-20125-1637 under strain rates of $2.67 \times 10^{-3}\ s^{-1}$ to $4500\ s^{-1}$, the stress–strain response can be described by a function comprising a rate-dependent modulus and a strain-dependent factor, while for PORON 4701-01-30125-1604 and 4701-12-30062-1604, only loading at high strain rates yields similar characteristics. Empirical equations were derived to characterize these mechanical properties; in addition, characteristics relating to energy-absorption capability as well as deformation under approximately constant stress were also studied. © 1997 John Wiley & Sons, Inc. J Appl Polym Sci **66:** 619–631, 1997

INTRODUCTION

High-density flexible polyurethane elastomers in sheet form are typical of soft materials used in many electronic products such as hand phones, calculators, and pagers to dissipate the otherwise destructive sudden changes in kinetic energy when these objects are subjected to unexpected impacts. To assess suitability for such applications, it is essential to first obtain their dynamic mechanical properties (loading and unloading stress–strain relationships) corresponding to different high strain rates. Such stress–strain curves are also very important to calculate cushion curves for packaging design.[1] In this study, three types of a flexible polyurethane elastomer in sheet form were selected for such characterization. The materials chosen are commercially produced for shock-absorption applications in electronic products. However, information on their behavior and performance under high-rate deformation is generally unspecified. The materials examined encompassed a range of flexibilities and densities, with their thicknesses also varying between 1.6 and 3.2 mm. Since the samples were thin, it was possible to induce very high strain rates even with low-velocity impacts by the striker in the test device. It is generally convenient to measure the stress–strain behavior of elastomers at low to medium strain rates of 10^{-4} to $10^{1}\ s^{-1}$ using screw-driven testing machines or gas-operated devices with a movable piston, which apply a constant strain rate.[2] High-velocity impact ($\dot{\varepsilon} \geq 10^{2}\ s^{-1}$) tests can be achieved by split

Correspondence to: V. P. W. Shim.

Contract grant sponsors: Motorola Electronics Pte. Ltd., Singapore; Singapore National Science and Technology Board.

Journal of Applied Polymer Science, Vol. 66, 619–631 (1997)

 CCC 0021-8995/97/040619-13

Hopkinson pressure bars (SHPB) and high-speed drop weight testers.[3,4] However, since stress wave effects must be considered at these high velocities, accuracy of experimental data, especially in the initial portion of stress–strain curves, are questionable because significant engineering strain is induced in soft specimens before the stress and strain in them attain a uniform state. Up to the present time, such problems in high-velocity tests remain unsolved and no further improvements have yet been proposed. Hence, a primary objective of this investigation was to devise a modified SHPB arrangement in which the striker, input, and output bars were made of polycarbonate instead of metal, thus improving the accuracy of stress–strain curves derived for soft materials at high strain rates. Wang et al.[5] undertook a theoretical analysis of using polymeric material in split Hopkinson bars; however, no practical applications of their analysis have been reported. The reason for using polycarbonate Hopkinson bars in the present study was to reduce mismatch in wave impedance between the input/output bars and the specimen; such mismatch leads to a large reflected wave from the interface between input bar and specimen. The large reflected wave results in a relatively long time required for the stress and strain within the specimen to reach an equilibrium state. Moreover, impedance mismatching also renders the transmitted signal too small to be accurately measured. Theoretical analysis in this investigation shows that replacement of the aluminum bars by polycarbonate ones can reduce significantly the time required for stress in the specimen to achieve equilibrium. Some typical stress–strain curves are presented and empirical equations derived to describe the dynamic properties of the three polyurethane elastomers studied.

EXPERIMENTAL

Three types of polyurethane foam in sheet foam, commonly used in electronic communication products, were studied—PORON 4701-01-30125-1604 (PORON A), which has a density of 480 kg/m^3 and a thickness of 3.2 mm; PORON 4701-12-30062-1604 (PORON B), with a density of 480 kg/m^3 and a thickness of 1.6 mm; and PORON 4701-05-20125-1637 (PORON C), with a density of 320 kg/m^3 and a thickness of 3.2 mm. These are microcellular materials with an average open cell size of 100 microns. Specimens for both quasi-static and dynamic compression were circular disks with respective diameters of 12.5 and 7.7 mm and were punched out from foam sheets. Quasi-static compression tests were performed using an Instron universal testing machine. The crosshead speed ranged from 0.5 to 100 mm/min, corresponding to strain rates of 2.67×10^{-3} s^{-1} to 5.34×10^{-1} s^{-1} for a 3.2 mm-thick specimen. The applied load and resulting deflection were recorded, from which corresponding quasi-static engineering stress–strain relationships were obtained.

Dynamic compression tests were performed using an SHPB apparatus[6] (Fig. 1). For this type of equipment, the time required to attain a uniform stress state in a specimen depends on both the mismatch in mechanical impedance (ρCA) between the bar and specimen and the specimen length. The elastic wave speed through foams is generally relatively small compared to wave speeds in metals. If both the input and output bars are metallic, it will take a considerable time for the stress in a specimen to reach equilibrium. During this time, significant engineering strain would have been induced, so that the initial portion of the stress–strain curve is not accurate. In this study, polycarbonate (LEXAN 141), which has a much smaller ρC (1.69×10^6 kg/m^{2}s) than that of 6061-T6 aluminum ($\rho C = 13.77 \times 10^6$ kg/m^{2}s) is used for the input, output, and striker rods to reduce the engineering strain induced in nonmetallic specimens before they achieved a uniform state of stress.

In Figure 1, the diameter of the striker and input/output bars is 10.5 mm, and the length for the striker, input, and output bars are chosen, respectively, to be 300, 1020, and 1020 mm. This results in an r/L ratio of 0.08 (r = the radius of input/output bars and L = length of incident pulse), which is smaller than 0.1, implying that geometrical dispersion effects need not be considered in this test. The gauges for measuring the incident and transmitted strains are bonded, respectively, 350 and 250 mm away from the specimen so that there is no signal superposition between the incident wave and that reflected from the specimen as well as between the transmitted wave and its own reflection from the free end. Another set of strain gauges is bonded on the input bar near the struck end, 510 mm away from the gauge measuring the incident strain.

Figure 2 shows that the incident strain pulses at these two locations on the input bar are almost identical, meaning that viscoelastic dispersion in the polycarbonate bar is negligible. The wave ve-

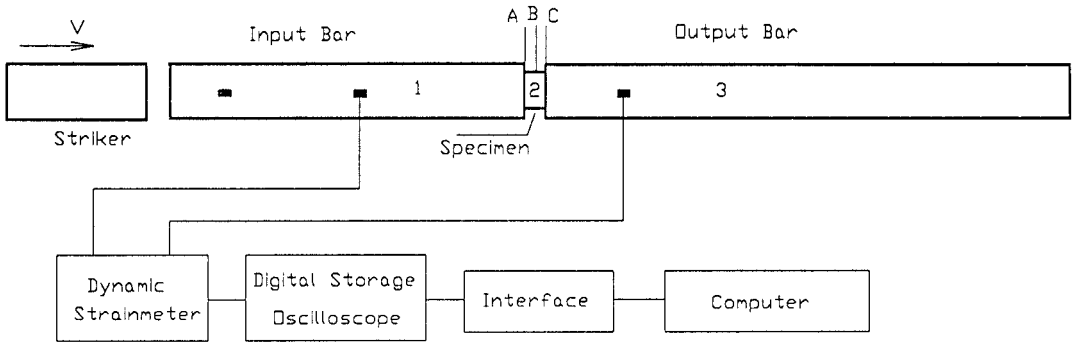

Figure 1 Split Hopkinson pressure bar.

locity in the polycarbonate bar was found to be 1490 m/s. Dynamic compressive stress–strain curves (Fig. 3) for polycarbonate (LEXAN 141), obtained from a metallic SHPB apparatus, also show the existence of an initial elastic response, implying that the stress wave propagated in the polycarbonate bars can be regarded as one-dimensional if its magnitude does not exceed yield. To quantify the effect of mechanical impedance mismatch on the time required for stress in a specimen to reach a uniform state, the propagation of a stress wave in an (aluminum bar)–(foam specimen)–(aluminium bar) configuration was analyzed and compared with a (polycarbonate bar)–(foam specimen)–(polycarbonate bar) arrangement.

With reference to Figure 4, the equations describing the reflected and transmitted stresses σ_r and σ_t at a boundary, in terms of the incident stress, σ_i, the cross-sectional areas A_1, and A_2, and the material properties ρ_1, ρ_2, E_1, and E_2, are given by

$$\tilde{\sigma}_r = \frac{\rho_2 C_2 A_2 - \rho_1 C_1 A_1}{\rho_2 C_2 A_2 + \rho_1 C_1 A_1}\,\tilde{\sigma}_i \tag{1}$$

$$\tilde{\sigma}_t = \frac{2\rho_2 C_2 A_1}{\rho_2 C_2 A_2 + \rho_1 C_1 A_1}\,\tilde{\sigma}_i \tag{2}$$

where ρ is the density and $C = \sqrt{E/\rho}$ is the elastic wave speed. Two cases are examined: Both the input and output bars are first assumed to be made of 6061-T6 aluminum alloy and then of polycarbonate (LEXAN 141). A small specimen of PORON A is considered to be inserted between the input and output bars. Both the 6061-T6 alu-

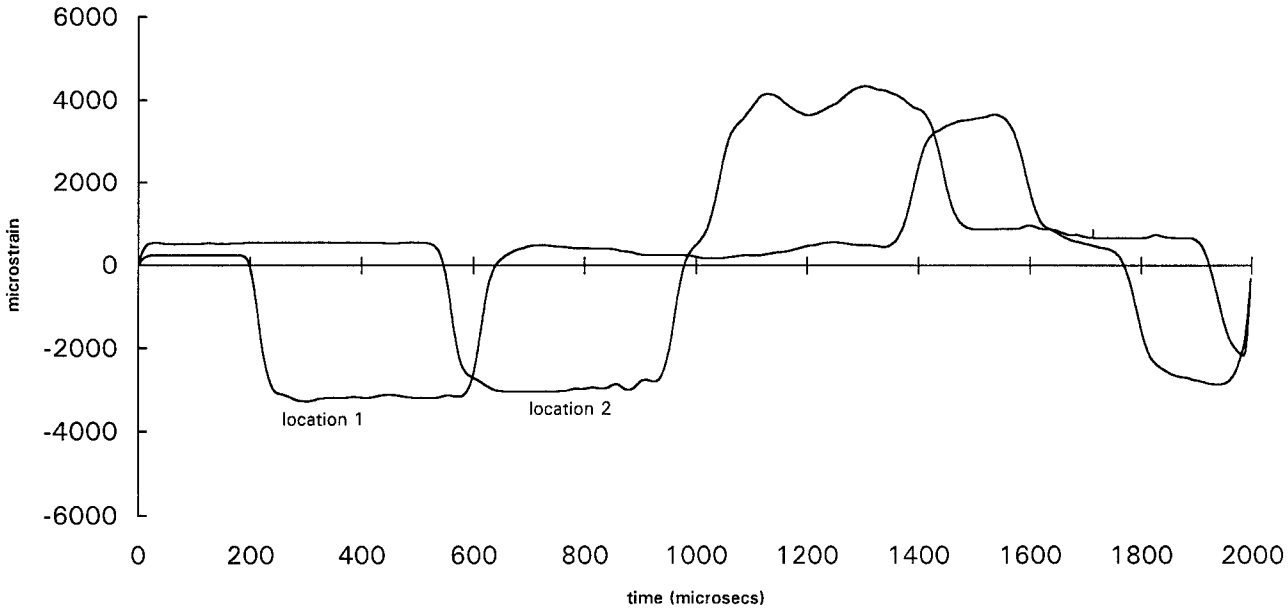

Figure 2 Incident wave forms at different locations on imput bar.

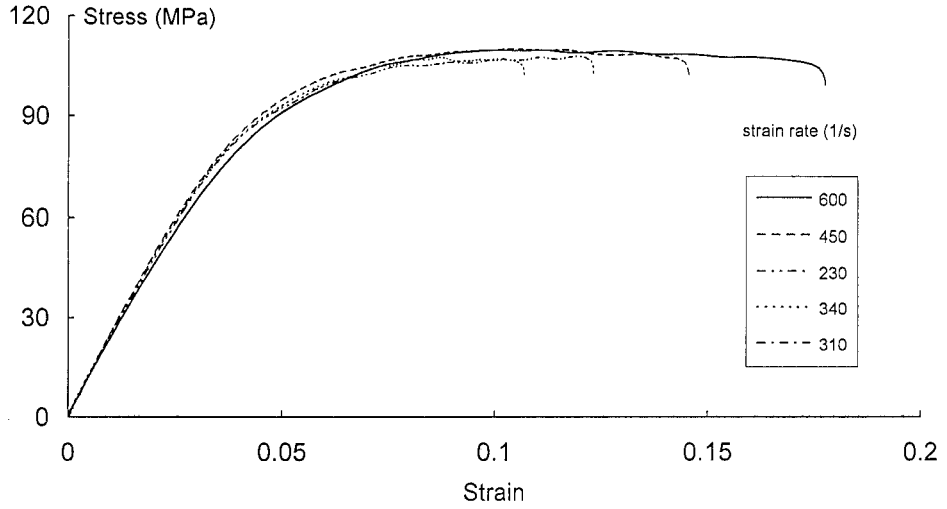

Figure 3 Dynamic compressive stress–strain curves for polycarbonate.

minum alloy and polycarbonate (LEXAN 141) were tested and found to be strain-rate-independent under compression. The initial elastic modulus of the 6061-T6 aluminum alloy and polycarbonate (LEXAN 141) are 70.0 and 2.45 GPa, respectively. PORON A has a density of 480 kg/m^3 and its elastic modulus varies with the strain rate; it is assumed to be 60.0 MPa in this analysis. The diameter of the input/output bars is 10.5 mm, while it is 7.6 mm for the specimen which is 3.2 mm long. To simplify the analysis of stress propagation through the input/output bars and specimen, it is assumed that the magnitude of the stress is sufficiently small for the foam to remain elastic during loading. By repeatedly applying eqs. (1) and (2) for transmission of stress between the input aluminum bar (material 1) and the PORON specimen (material 2) (see Fig. 1), the transmitted and reflected stresses are

$$\tilde{\sigma}_t = 0.0245\sigma_i \tag{3a}$$

$$\tilde{\sigma}_r = -0.9848\sigma_i \tag{3b}$$

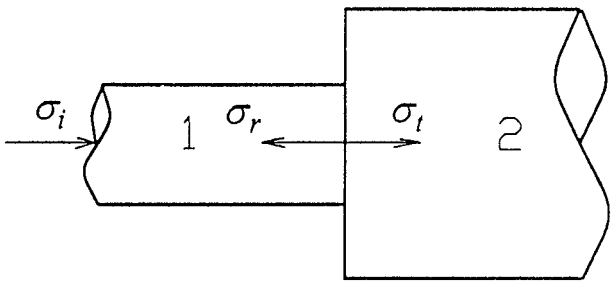

Figure 4 Propagation of stress across a boundary.

Hence,

$$\sigma_1^1 = \tilde{\sigma}_i + \tilde{\sigma}_r = 0.0152\sigma_i \tag{4a}$$

$$\sigma_2^1 = \tilde{\sigma}_t = 0.0245\sigma_i \tag{4b}$$

where σ_1^1 and σ_2^1 are the first stepwise changes in stress in materials 1 and 2, respectively. Between the PORON specimen (material 2) and the output aluminum bar (material 3), the stress transmitted to the output bar is

$$\tilde{\sigma}_t = \frac{2\rho_3 C_3 A_2}{\rho_3 C_3 A_3 + \rho_2 C_2 A_2}\,\sigma_2^1 = C_t\sigma_2^1 \tag{5}$$

while the stress reflected back into the specimen is

$$\tilde{\sigma}_r = \frac{\rho_3 C_3 A_3 - \rho_2 C_2 A_2}{\rho_3 C_3 A_3 + \rho_2 C_2 A_2}\,\sigma_2^1 = C_r\sigma_2^1 \tag{6}$$

where C_t and C_r are defined, respectively, as the transmission and reflection coefficients for stress from the specimen to the input/output bars. For stress propagating from the PORON specimen to an aluminum bar, $C_t = 1.2306$ and $C_r = 0.9848$.

Therefore,

$$\sigma_2^2 = \sigma_2^1 + C_r\sigma_2^1 = 0.0245\sigma_i(1 + C_r) \tag{7a}$$

$$\sigma_3^1 = 0.0245\sigma_i C_t \tag{7b}$$

where σ_2^2 is the second stepwise change in stress in material 2 and σ_3^1 is the first stepwise change in stress in material 3. From the PORON speci-

men (material 2) to the aluminum input bar (material 1),

$$\tilde{\sigma}_t = \frac{2\rho_1 C_1 A_2}{\rho_1 C_1 A_1 + \rho_2 C_2 A_2} C_r \sigma_2^1 = C_t C_r \sigma_2^1 \quad (8)$$

$$\tilde{\sigma}_r = \frac{\rho_1 C_1 A_1 - \rho_2 C_2 A_2}{\rho_1 C_1 A_1 + \rho_2 C_2 A_2} C_r \sigma_2^1 = C_r^2 \sigma_2^1 \quad (9)$$

Hence, the stress in material 2 after the third stepwise change and the stress in material 1 after the second stepwise change are given by

$$\sigma_2^3 = 0.0245\sigma_i(1 + C_r + C_r^2) \quad (10a)$$

$$\sigma_1^2 = (1 - C_r)\sigma_i + C_r C_t \sigma_2^1 \quad (10b)$$

Note that the stresses in the input bar, specimen, and output bar increase according to the stepwise fashion described. The time interval for each stress level in the specimen is $\Delta t = (L_{\text{specimen}}/C_{\text{specimen}}) = 9.0\ \mu$s. However, the corresponding time interval for each stress level in the input and output bars at their interface with the specimen is $2\Delta t$ (18.0 μs). The stresses in the input bar, specimen, and output bar after the nth step ($t = n\Delta t$) are

$$\sigma_1^n = (1 - C_r)\sigma_i + C_r C_t \sigma_2^1 (1 + C_r^2 + (C_r^2)^2 + \cdots + (C_r^2)^{n-2}) = (1 - C_r)\sigma_i + C_r C_t \sigma_2^1 \times \frac{1 - (C_r^2)^{n-1}}{1 - C_r^2} \quad (n \geq 2) \quad (11)$$

$$\sigma_2^n = \sigma_2^1 (1 + C_r + C_r^2 + C_r^3 + \cdots C_r^{n-1}) = \sigma_2^1 \times \frac{1 - C_r^n}{1 - C_r} \quad (n \geq 1) \quad (12)$$

$$\sigma_3^n = C_t \sigma_2^1 (1 + C_r^2 + (C_r^2)^2 + \cdots + (C_r^2)^{n-1}) = C_t \sigma_2^1 \times \frac{1 - (C_r^2)^n}{1 - C_r^2} \quad (n \geq 1) \quad (13)$$

Equations (11)–(13) are general and also apply to polycarbonate input/output bars, with $C_r = 0.884$, $C_t = 1.168$, and $\sigma_2^1 = 0.1866\sigma_i$. Figure 5 shows the stress history at A, B, and C (Fig. 1) for a polycarbonate–foam–polycarbonate configuration. Since the cross-sectional area of the input/output bars is 1.6 times that of the specimen, σ_B in Figure 5 is normalized with respect to $1.6\sigma_i$, while both σ_A and σ_C are normalized with respect to σ_i. The results show that the stress at surfaces A and C attain approximate equilibrium after 8 steps (144.0 μs), implying that stress in the specimen becomes essentially uniform at that time. In contrast, eqs. (11)–(13) show that for aluminum input/output bars it will take about 100 time steps (900.0 μs) for stress in a specimen to reach a uniform state. It becomes obvious that the use of polycarbonate for the input/output bars greatly reduces the time required for soft material specimens to reach a uniform stress state. The stress, strain, and strain rate in a specimen as functions of time are described by

$$\sigma(t) = \frac{E_0 A_0}{2A_s}(\varepsilon_i + \varepsilon_r + \varepsilon_t) \quad (14)$$

$$\varepsilon(t) = \frac{C_0}{l_0}\int_0^t [\varepsilon_i(\tau) - \varepsilon_r(\tau) - \varepsilon_t(\tau)]\, d\tau \quad (15)$$

$$\dot{\varepsilon}(t) = \frac{C_0}{l_0}[\varepsilon_i(t) - \varepsilon_r(t) - \varepsilon_t(t)] \quad (16)$$

where ε_i is the strain in the input bar; ε_r, the strain reflected from the interface with the specimen; and ε_t, the strain induced in the output bar. A_0 and A_s are, respectively, the cross-sectional areas of the input/output bars and the specimen; E_0 and C_0 are the elastic modulus and the elastic wave velocity of the input/output bar material. When the stress within a specimen has reached a uniform state, eqs. (14)–(16) can be simplified to

$$\sigma(t) = \frac{E_0 A_0}{A_s}\varepsilon_t(t) \quad (17)$$

$$\varepsilon(t) = \frac{2C_0}{l_0}\int_0^t [\varepsilon_i(\tau) - \varepsilon_t(\tau)]\, d\tau \quad (18)$$

$$\dot{\varepsilon}(t) = \frac{2C_0}{l_0}[\varepsilon_i(t) - \varepsilon_t(t)] \quad (19)$$

Figure 6 shows typical signals of incident, reflected, and transmitted waves obtained from dynamic compression of PORON A.

RESULTS AND DISCUSSION

In quasi-static compression tests, a triaxial stress state may develop in the thin disk specimens used although friction between a specimen and the loading faces is minimized by applying grease on the interfaces. Hence, the stress–strain curves obtained may not be totally accurate and should only be used primarily for comparison with dynamic test results. For homogeneous specimens

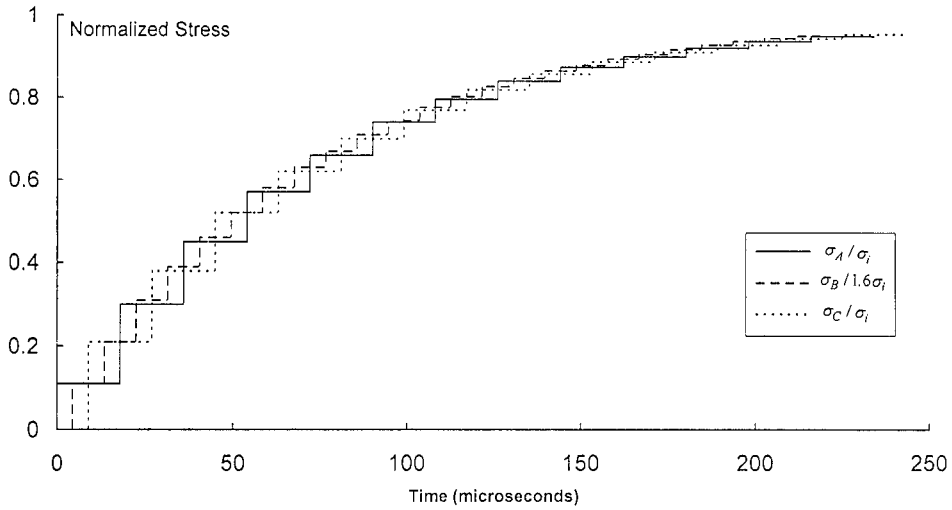

Figure 5 Stress history at A, B, and C.

in SHPB tests, the DAVIES and HUNTER (D/H)[7] criterion has to be satisfied, i.e., the ratio L/D (L and D are, respectively, the length and diameter of the specimen) must lie between 0.5 and 1.0. However, for microporous or microcellular materials such as the foam under study, it is almost impossible to derive a similar criterion from theoretical analysis. In this investigation, experiments were conducted to examine the effects of specimen size on the results obtained. Stress–strain curves for specimens of different length/diameter ratios are shown in Figure 7. It was found that the maximum difference between any two of the three curves is less than 8.0% for specimen length/diameter ratios varying from 0.32 to 0.6.

Experiments show that apart from a mismatch in mechanical impedance, the strain rate also has an effect on the time required for a specimen to attain a uniform stress state. For a given strain rate, the forces at the two ends of a specimen can be obtained from the incident, reflected, and transmitted waves:

$$P_1 = A_0E_0(\varepsilon_i + \varepsilon_r) \tag{20}$$

$$P_2 = A_0E_0\varepsilon_t \tag{21}$$

Figure 8 shows the force histories P_1 and P_2 at the ends of PORON A specimens loaded at three different strain rates. From these curves, it is found that P_1, the force exerted by the input bar, is initially larger than P_2, the force between the specimen and the output bar. This situation con-

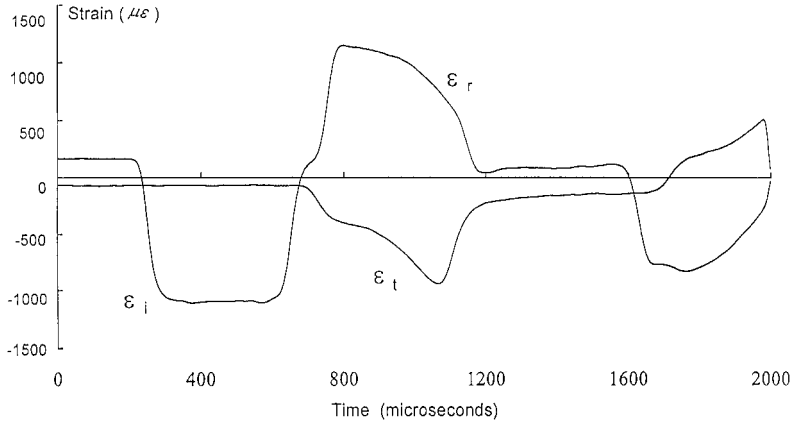

Figure 6 Typical incident, reflected, and transmitted strain signals for PORON A.

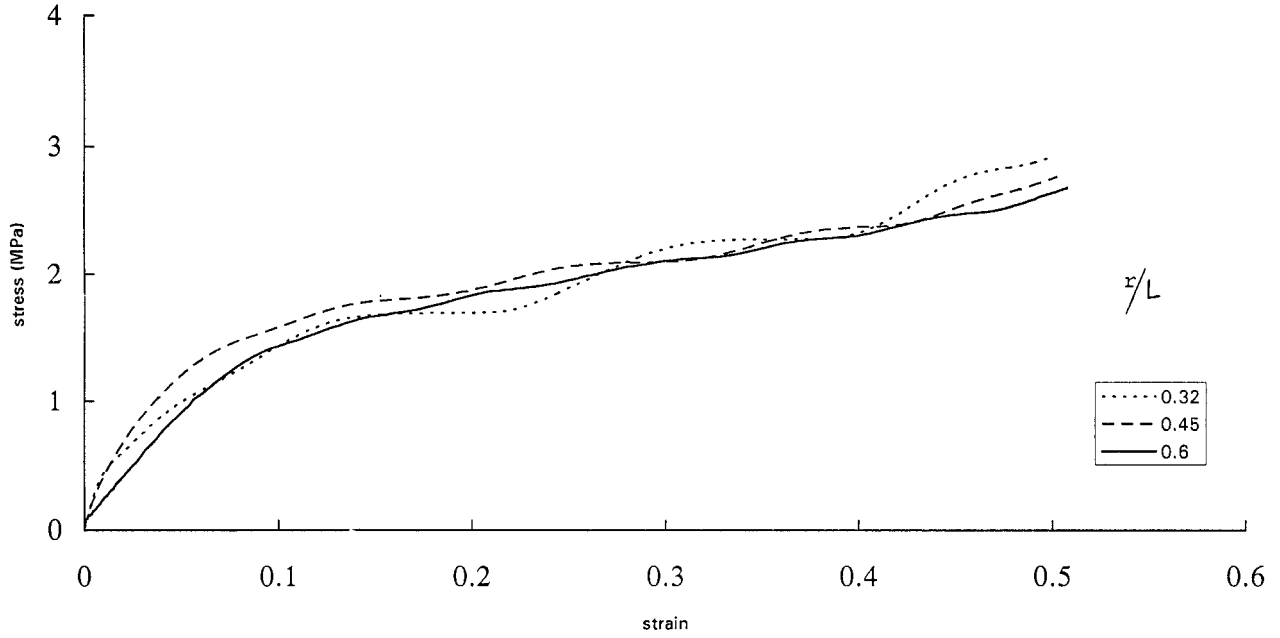

Figure 7 Specimen size effects on the dynamic stress–strain curves.

tinues until a point in time (E), after which P_1 and P_2 are almost equal. The engineering strain induced in the specimen before point E (ε_E) as well as the time corresponding to this (t_E) are listed in Table I. At a higher strain rate, a larger engineering strain is induced before point E is reached, although a shorter time is required for stress in the specimen to reach equilibrium. Similar results were also obtained for PORON B and PORON C.

In terms of utilizing the materials studied in shock attenuation and impact energy-absorption applications, a knowledge of their compressive loading and unloading stress–strain curves (hysteresis loops) is necessary. The larger the area enclosed in a dynamic loading–unloading loop, the higher the capacity for energy absorption. In this study, quasi-static and dynamic loading–unloading stress–strain curves were examined. Figures 9–11 depict the engineering stress–engineering strain curves for PORON A, B, and C, respectively, under dynamic compression. As is typical of cellular materials and structures, the loading portion comprises an initial linear elastic response, an extended postyield plateaulike phase, and a final steep increase in stress as collapsed cells are compacted together.[8–10] It is noted that for the dynamic stress–strain curves shown in Figures 9–11 the strain rate during the entire deformation is not absolutely constant. It is almost constant in the plateau phase, but drops quickly after that and momentarily reaches zero value at the maximum strain point. The strain rates stated in Figures 9–11 are the average values during the entire deformation. These results indicate that the three types of PORON exhibit rate-sensitive behavior. An increase in strain rate is accompanied by an increase in the initial modulus, yield strength, and stress level for a given strain. (Yield stress is defined as the stress corresponding to the intersection of the extensions of the initial linear portion and the plateau phase.) After yield, when cells within the material begin to buckle and collapse, all the foams under investigation exhibit a plateaulike response in which the stress increases very gradually before culmi-

Table I

Strain Rate $\dot{\varepsilon}$ (s^{-1})	t_E (μs)	ε_E (%)
610	115.6	7.05
1820	82.6	15.03
2630	71.6	18.82

Time and strain induced when forces at specimen ends attain eqality.

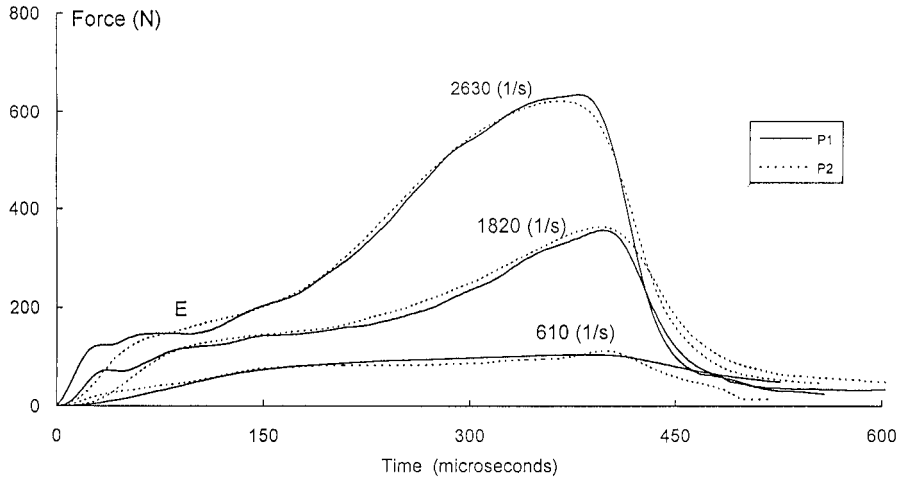

Figure 8 Load histories at ends of PORON A specimens.

nating in a final steep increase; this is followed by viscoelastic recovery during unloading, after attainment of maximum strain.

Under dynamic compression, the maximum strain induced is controlled by the duration of the incident stress pulse. Since the length of the incident stress wave was kept constant because of a fixed striker length, a higher strain rate results in a larger strain being induced in a specimen. Following compression at high strain rates, the specimen dimensions were measured and it was found that the specimens exhibited almost complete recovery, but only after several minutes, which is much longer than the loading time. Since the input and output bars are of finite length, stress waves returning from their free ends will interfere with the incident, transmitted, and reflected waves; thus, the full recovery process could not be recorded. Hence, the portions of the stress–strain curves after point P in Figures 9–11 were

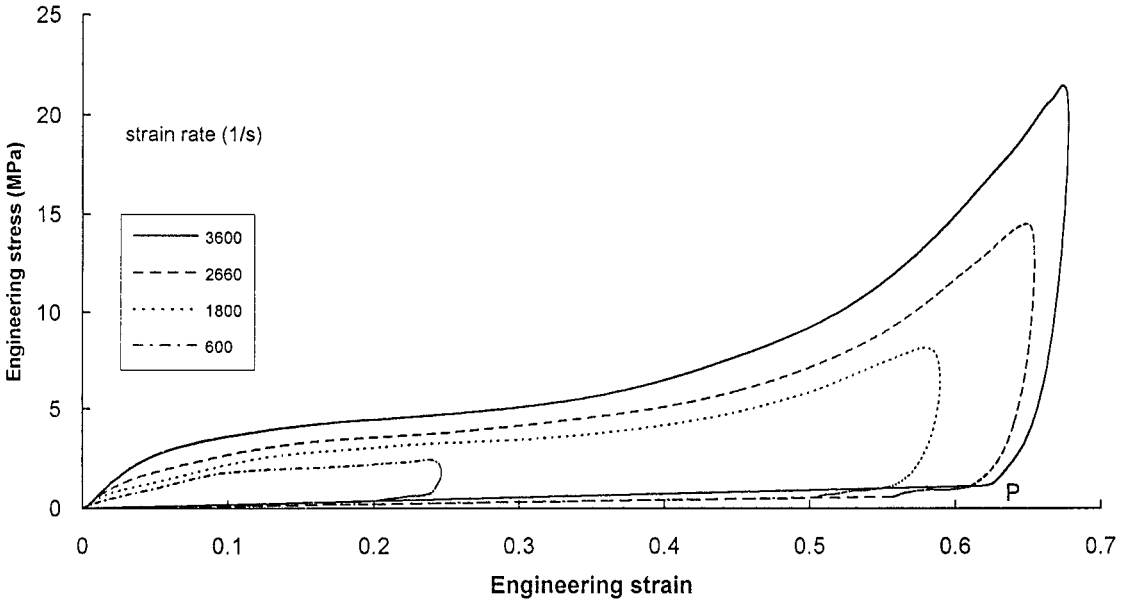

Figure 9 Dynamic compressive stress–strain curves for PORON A.

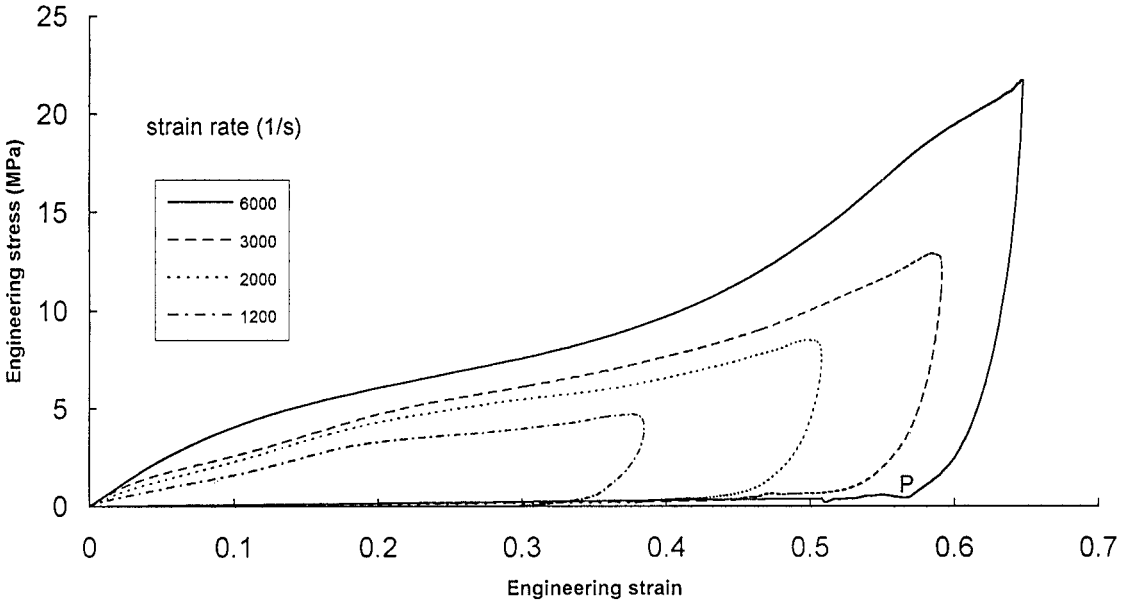

Figure 10 Dynamic compressive stress–strain curves for PORON B.

obtained by extrapolating the recorded data back to the origin. The initial modulus (E_0) and yield strength (σ_y) of the three foams at different strain rates are shown in Figures 12 and 13, respectively. It was found that under both quasi-static and dynamic compression, the initial modulus, and yield strength of the three foams can be described approximately by bilinear functions of the form

$$E_0 = \begin{cases} a_0 + b_0 \ln \dot{\varepsilon}; & \ln \dot{\varepsilon} \le 5.5 \\ a_1 + b_1 \ln \dot{\varepsilon}; & \ln \dot{\varepsilon} \ge 5.5 \end{cases} \quad (22)$$

$$\sigma_y = \begin{cases} c_0 + d_0 \ln \dot{\varepsilon}; & \ln \dot{\varepsilon} \le 5.5 \\ c_1 + d_1 \ln \dot{\varepsilon}; & \ln \dot{\varepsilon} \ge 5.5 \end{cases} \quad (23)$$

where a_0, b_0, a_1, b_1, c_0, d_0, c_1, and d_1 are con-

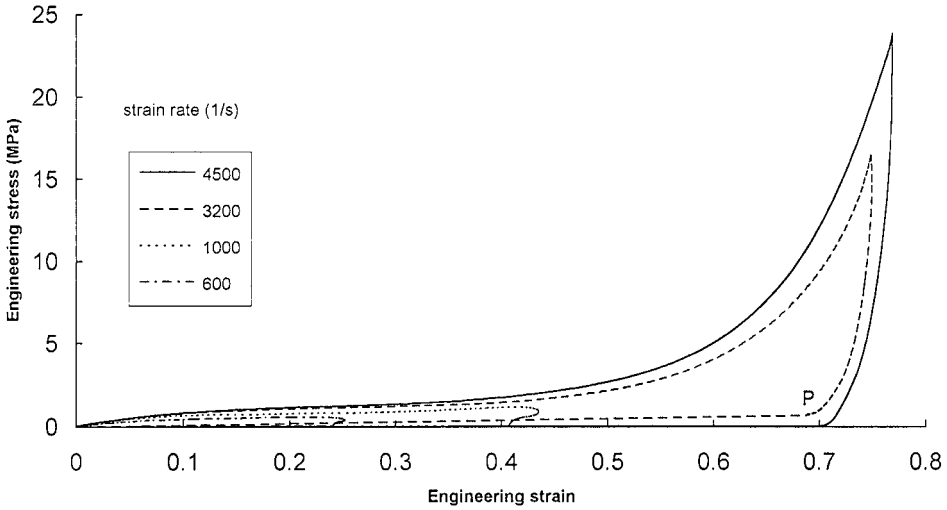

Figure 11 Dynamic compressive stress–strain curves for PORON C.

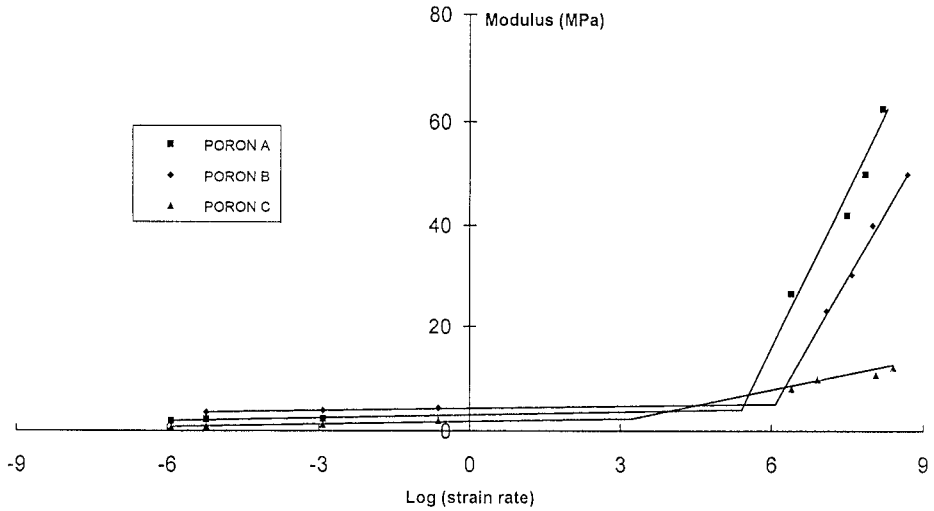

Figure 12 Variation of initial modulus with strain rate.

stants. Figures 12 and 13 depict experimental data on how E_0 and σ_y vary with strain rate. Segmented linear fits of the data points show that the behavior of E_0 and σ_y fall roughly into two distinct regimes of linearity. The slopes of the lines for dynamic compression are much higher than those for quasi-static deformation. It appears that there exists a transition strain rate corresponding to $\ln \dot{\varepsilon} \approx 5.5$, above which the initial modulus and yield strength increase very rapidly.

For the purpose of both stress analysis and material utilization, it would be ideal if stress–strain data for all strain rates were available. As such comprehensive information is generally not possible to collect, it would therefore be useful to be able to derive a good estimate of the stress–strain behavior at any strain rate based on limited experimental data. To achieve this, the loading portion of each stress–strain curve is normalized with respect to its initial modulus. The normalized stress–strain curves for the three types of

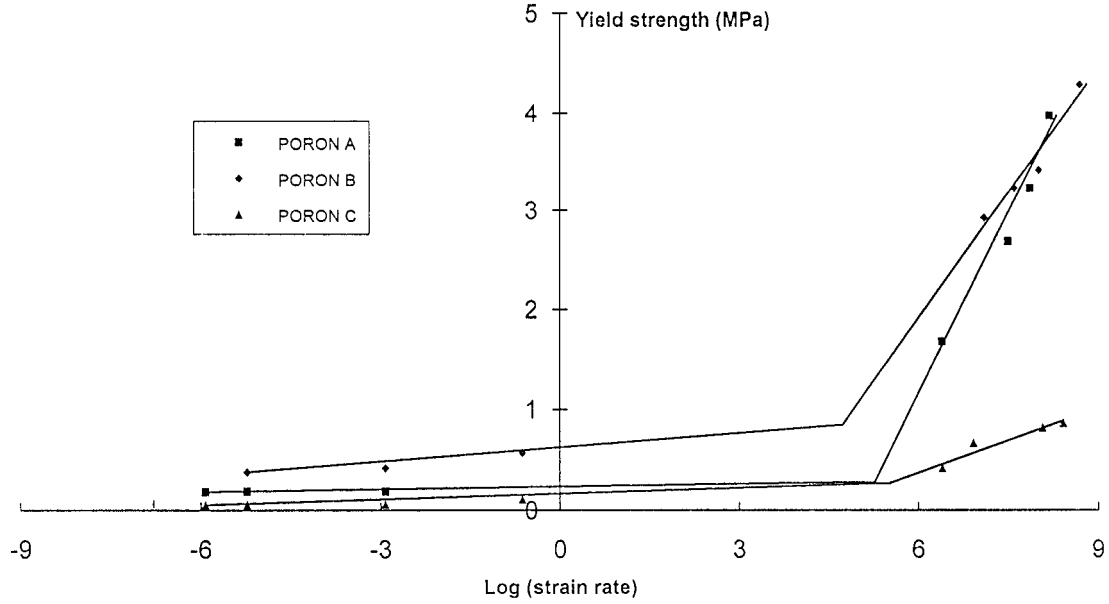

Figure 13 Variation of yield strength of strain rate.

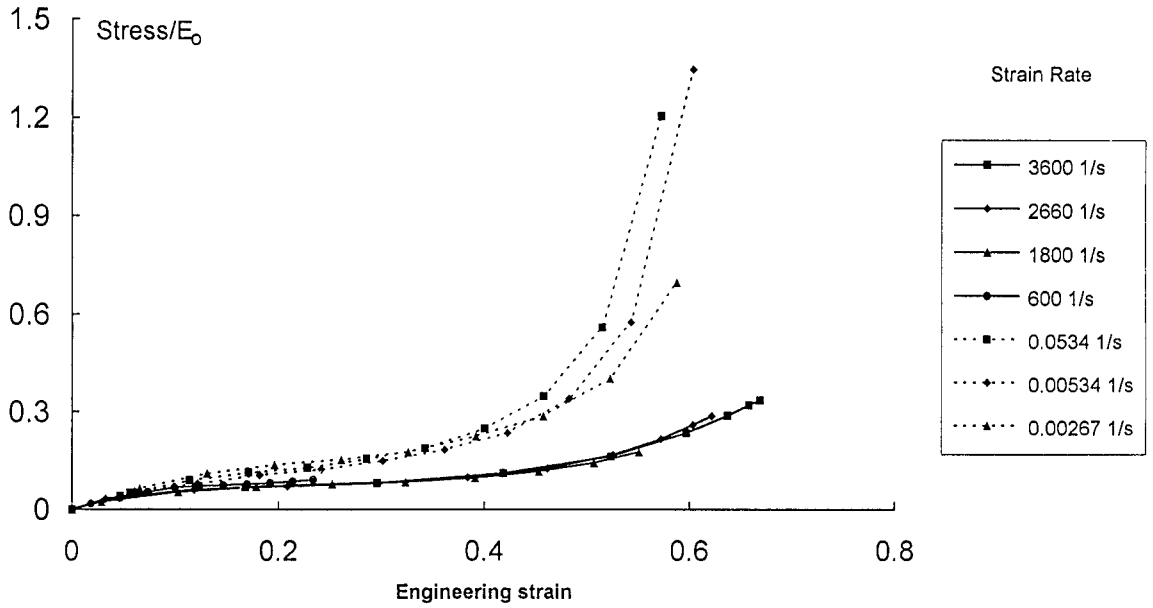

Figure 14 Normalized stress–strain curves for PORON A.

foam under both quasi-static and dynamic compression are shown in Figures 14–16. It was found that for both quasi-static and dynamic compression the normalized stress–strain curves for PORON C collapse approximately into a single curve. However, PORON A and PORON B only exhibit this characteristic under dynamic compression. This feature provides a means of conveniently characterizing stress–strain properties at different strain rates. It is proposed that the loading stress be described by a function comprising the product of a rate-dependent modulus factor and a strain-dependent factor:

$$\sigma = E_0(\dot{\varepsilon})f(\varepsilon) \tag{24}$$

where E_0 is the experimentally obtained initial modulus which can be defined as a function of strain rate; $f(\varepsilon)$ can also be determined from the

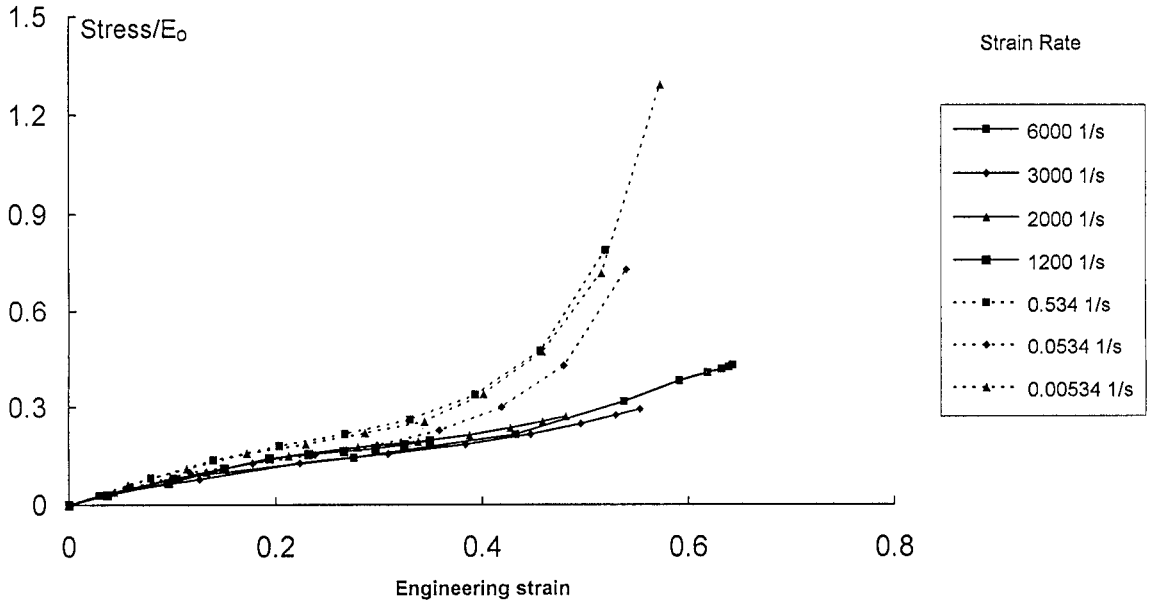

Figure 15 Normalized stress–strain curves for PORON B.

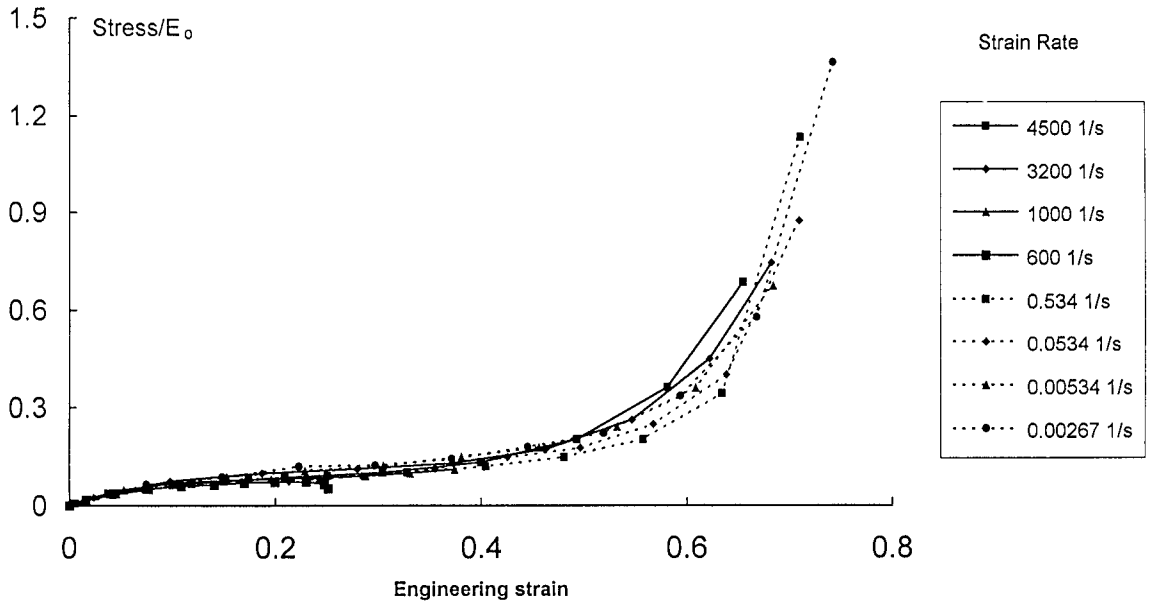

Figure 16 Normalized stress–strain curves for PORON C.

normalized stress–strain curves. The general form of eq. (24) may be deduced by examining the characteristics of the components $E_0(\dot{\varepsilon})$ and $f(\varepsilon)$. From eq. (22) and Figures 14–16, the initial modulus follows an approximate bilinear function of $\ln \dot{\varepsilon}$, while $f(\varepsilon)$ is found to conform to a polynomial of at least fourth order. A combination of these descriptions of $E_0(\dot{\varepsilon})$ and $f(\varepsilon)$ yields the general form of eq. (24) as

$$\sigma = [A_0 + A_1 \ln \dot{\varepsilon}] \times (B_0 + B_1\varepsilon + B_2\varepsilon^2 + B_3\varepsilon^3 + B_4\varepsilon^4 + \cdots + B_n\varepsilon^n) \quad (25)$$

By employing the above equation, the dynamic compressive stress–strain relationship for PORON A under strain rates ranging from 600 to 3600 s^{-1} can be described by

$$\sigma = [-94.86 + 18.71 \ln \dot{\varepsilon}] \times (0.8268\varepsilon - 3.4071\varepsilon^2 + 5.6431\varepsilon^3 - 1.9355\varepsilon^4) \quad (26)$$

where $600 \le \dot{\varepsilon} \le 3600\ s^{-1}$

For PORON B,

$$\sigma = [-98.65 + 17.14 \ln \dot{\varepsilon}](1.409\varepsilon - 6.237\varepsilon^2 + 13.285\varepsilon^3 - 8.324\varepsilon^4) \quad (27)$$

where $1200 \le \dot{\varepsilon} \le 6000\ s^{-1}$

For PORON C,

$$\sigma = [-2.38 + 1.68 \ln \dot{\varepsilon}] \times (0.0398 - 1.86\varepsilon + 37.76\varepsilon^2 - 251.96\varepsilon^3 + 756.25\varepsilon^4 - 1042.74\varepsilon + 540.11\varepsilon^6)^5 \quad (28a)$$

where $300 \le \dot{\varepsilon} \le 4500\ s^{-1}$

$$\sigma = [2.05 + 0.22 \ln \dot{\varepsilon}] \times (0.0398 - 1.86\varepsilon + 37.76\varepsilon^2 - 251.96\varepsilon^3 + 756.25\varepsilon^4 - 1042.74\varepsilon^5 + 540.11\varepsilon^6) \quad (28b)$$

where $0.534 \le \dot{\varepsilon} \le 300\ s^{-1}$

A comparison between the proposed stress–strain curves and experimental results for PORON C in Figure 17 shows that eqs. (28a) and (28b) are useful for estimating stress–strain behavior at strain rates which are difficult to induce exactly in experiments. For example, the predicted stress–strain curves for strain rates of 2.67×10^{-3} and 600 s^{-1} are shown together with the experimental results.

CONCLUSIONS

(a) The use of polycarbonate in place of metal for the input, output, and striker bars of a

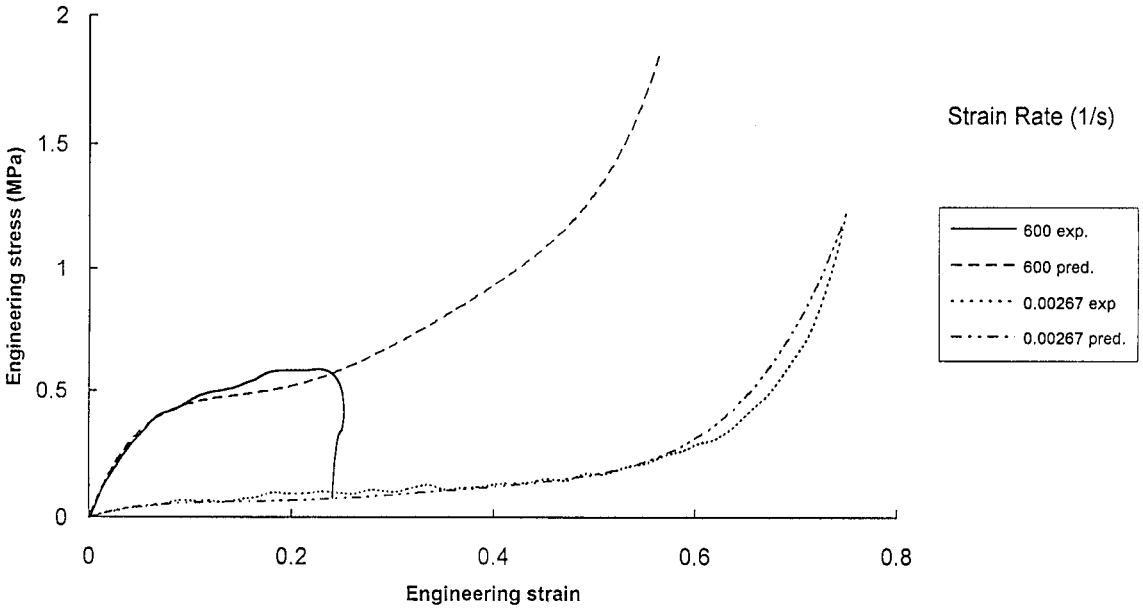

Figure 17 Measured and predicted engineering stress–strain curves for PORON C.

split Hopkinson pressure bar device reduces mismatch in mechanical impedance with more compliant, nonmetallic test specimens such as flexible polyurethane foam and facilitates enhanced accuracy in determination of their dynamic stress–strain characteristics.

(b) The foams examined, which are used in shock-absorption applications inside electronic products, are highly strain rate-dependent. Both the initial modulus and yield stress can be described by linear functions of log strain rate for both quasi-static and dynamic compression. Test results indicate the existence of a transition strain rate regime, whereby deformation at more rapid rates increases the initial modulus and yield stress sharply.

(c) For PORON C deformed at strain rates of 2.67×10^{-3} to 4500 s^{-1}, the loading stress can be described by a function comprising a rate-dependent initial modulus and a strain-dependent function. The behavior of PORON A and PORON B at high strain rates also conforms to a function of similar form.

The authors wish to acknowledge Motorola Electronics Pte. Ltd. (Singapore) and the Singapore National Science and Technology Board for their support in this investigation.

REFERENCES

1. N. G. Hilyard and A. Cunningham, *Low Density Cellular Plastics,* Chapman and Hall, London, 1994.
2. S. J. Green, F. L. Schierloh, R. D. Perkins, and S. G. Babcock, *Exp. Mech.,* **9,** 103–109 (1969).
3. J. A. Rinde and K. G. Hoge, *J. Appl. Polym. Sci.,* **15,** 1377–1395 (1971).
4. A. Gale and N. J. Mills, *Plast. Rubb. Process. Appl.,* **5,** 101–108 (1985).
5. L. Wang, K. Labibes, Z. Azari, and G. Pluvinage, *Int. J. Impact Eng.,* **15,** 669–686 (1994).
6. H. Kolsky, *Proc. Phys. Soc. (Lond.),* **62-B,** 676–700 (1949).
7. E. D. H. Davies and S. C. Hunter, *J. Mech. Phys. Solids,* **11,** 155 (1963).
8. L. J. Gibson and M. F. Ashby, *Cellular Solids,* Pergamon Press, Oxford, 1988.
9. V. P. W. Shim and W. J. Stronge, *Int. J. Mech. Sci.,* **28,** 683–707 (1986).
10. V. P. W. Shim, B. Y. Tay, and W. J. Stronge, *Trans. ASME J. Eng. Mater. Tech.,* **112,** 398–405 (1990).